Geosci. Model Dev., 10, 927–944, 2017
www.geosci-model-dev.net/10/927/2017/
doi:10.5194/gmd-10-927-2017

Geoscientific Model Development
Open Access
EGU

Aerosol–radiation interaction modelling using online coupling between the WRF 3.7.1 meteorological model and the CHIMERE 2016 chemistry-transport model, through the OASIS3-MCT coupler

Régis Briant[1,2], Paolo Tuccella[1], Adrien Deroubaix[1], Dmitry Khvorostyanov[1], Laurent Menut[1], Sylvain Mailler[1], and Solène Turquety[1]

[1]LMD, Laboratoire de météorologie dynamique, École Polytechnique, 91128 Palaiseau, France
[2]Climatic Change and Climate Impacts, Institute for Environmental Sciences, University of Geneva, Boulevard Carl-Vogt 66, 1205 Geneva, Switzerland

Correspondence to: Régis Briant (rbriant@lmd.polytechnique.fr)

Received: 1 April 2016 – Discussion started: 26 April 2016
Revised: 20 December 2016 – Accepted: 1 February 2017 – Published: 23 February 2017

Abstract. The presence of airborne aerosols affects the meteorology as it induces a perturbation in the radiation budget, the number of cloud condensation nuclei and the cloud micro-physics. Those effects are difficult to model at regional scale as regional chemistry-transport models are usually driven by a distinct meteorological model or data. In this paper, the coupling of the CHIMERE chemistry-transport model with the WRF meteorological model using the OASIS3-MCT coupler is presented. WRF meteorological fields along with CHIMERE aerosol optical properties are exchanged through the coupler at a high frequency in order to model the aerosol–radiation interactions. The WRF-CHIMERE online model has a higher computational burden than both models run separately in offline mode (up to 42 % higher). This is mainly due to some additional computations made within the models such as more frequent calls to meteorology treatment routines or calls to optical properties computation routines. On the other hand, the overall time required to perform the OASIS3-MCT exchanges is not significant compared to the total duration of the simulations. The impact of the coupling is evaluated on a case study over Europe, northern Africa, the Middle East and western Asia during the summer of 2012, through comparisons of the offline and two online simulations (with and without the aerosol optical properties feedback) to observations of temperature, aerosol optical depth (AOD) and surface PM_{10} (particulate matter with diameters lower than 10 µm) concentrations. The result shows that using the optical properties feedback induces a radiative forcing (average forcing of $-4.8\,W\,m^{-2}$) which creates a perturbation in the average surface temperatures over desert areas (up to 2.6° locally) along with an increase in both AOD and PM_{10} concentrations.

1 Introduction

Both the direct and semi-direct aerosol effects refer to the perturbation of the radiation budget induced by the presence of aerosol in the atmosphere along with the induced changes in the meteorology (e.g. surface temperature, wind velocity, cloud coverage) (Jacobson et al., 2007; Hansen et al., 1997). The indirect aerosol effects refer to changes in the number of cloud condensation nuclei along with the induced perturbations within the cloud micro-physics, and thus of the cloud albedo and precipitation (Jones et al., 1994). The aerosol effect processes are known to have a significant impact on meteorology and on airborne aerosol concentrations (Yu et al., 2006). However, aerosol effects are difficult to model precisely as studies focusing on chemistry and meteorology usually involve two distinct models. Hence, they are neglected or simplified through a climatology by offline models, as they are not capable of taking aerosol feedbacks into account. Developing fully coupled online models able to accurately take aerosol effects into account is a major scientific challenge (Zhang, 2008).

An online modelling approach enables the possibility of several models to be run concurrently and allows them to communicate with each other. Thus, it creates the possibility of feedback modelling, as models may interact both ways at each time step. Online models coupling meteorological models and chemistry-transport models (CTMs) are increasingly used (Baklanov et al., 2014). Merging two models in order to form a unique model is one solution (e.g. WRF-CHEM (Grell et al., 2005), CMCC-CESM-NEMO (Fogli and Iovino, 2014), IFS-ECWAM-NEMO (Breivik et al., 2015)). With this method all variables are shared; however, once models are merged it may be difficult to make each model component evolve independently. This is an issue when several independent modelling teams are involved or when more than two models are coupled. Using an external coupler to handle the variable exchanges is an alternative. Each model is interfaced with the coupler, allowing them to retain their independent course of development. The coupler may perform some operations on the coupling fields, such as interpolations. This approach is also a manner of sharing new model developments among research groups while allowing each group to continue to administrate their own model. This approach has been applied to several online coupling platforms such as WRF-CMAQ (Wong et al., 2012), CNRM-CM5 (Voldoire et al., 2013) or MPI-ESM (Giorgetta et al., 2013; Jungclaus et al., 2013).

OASIS is a widely used external coupler developed by the CERFACS (Centre Européen de Recherche et de Formation Avancée en Calcul Scientifique, Toulouse, France) (Valcke et al., 2015). Several geoscience models such as ECHAM (Stevens et al., 2013), LMDz (Hourdin et al., 2006) or ORCHIDEE (Krinner et al., 2005) have been interfaced with OASIS and, therefore, the OASIS coupler is used in several online models, such as EC-earth (Sterl et al., 2012), TerrSysMP (Gasper et al., 2014; Shrestha et al., 2014), the Met Office Unified Model (Williams et al., 2015) or IPSL-CM5 (Dufresne et al., 2013).

Several online-coupled regional air quality models have been developed (Im et al., 2015b) and many studies focused on the aerosol radiative impacts. Pérez et al. (2006) studied the interaction between mineral dust and solar radiation through the inclusion of mineral dust radiative effects within the DREAM regional atmospheric dust model (Nickovic et al., 2001). The feedback attributed to mineral dust is negative, with a 35–45 % reduction of the aerosol optical depth (AOD) over the Mediterranean region during a major mineral dust outbreak. Vogel et al. (2009) used the COSMO-ART fully online-coupled model over western Europe and showed that aerosol particles induce an average decrease in the 2 m temperatures (0.1 K over Germany). Han et al. (2012) showed that mineral dust particles induce a decrease of up to $90\,\mathrm{W\,m^{-2}}$ in long-wave radiative forcing along with an increase of $40\,\mathrm{W\,m^{-2}}$ in short-wave radiative forcing when using the RIEMS-Chemaero online regional climate–chemistry–aerosol model over eastern Asia.

In Péré et al. (2011), aerosol radiative effects over Europe are evaluated using both the Weather Research and Forecasting (WRF) meteorological model (Skamarock et al., 2007) and the CHIMERE regional chemistry-transport model (Schmidt et al., 2001; Bessagnet et al., 2004; Menut et al., 2013). Results indicate that the presence of particles induces perturbations in both the solar radiation (radiative forcing at the bottom of the atmosphere of -30 to $-10\,\mathrm{W\,m^{-2}}$) and the near-surface temperatures (decrease of up to 0.30 ± 0.06 K). An offline coupling was made by forcing the WRF model with aerosol optical properties computed from CHIMERE outputs. Initially, the CHIMERE model was forced by the WRF model itself, thereby implying the need to develop interactions between the two models. The WRF model was recently interfaced with the OASIS coupler (Valcke et al., 2015) and coupled online to the NEMO (Nucleus for European Modelling of the Ocean) ocean model (Madec, 2008) in order to better study air–sea interactions (Samson et al., 2014). On the other hand, recent developments within the CHIMERE CTM, made for the CHIMERE2016a (Mailler et al., 2016b) release, were related to the development of an online version of the CHIMERE model. These developments have been pursued, leading to the creation of an OASIS interface within the CHIMERE model. A WRF-CHIMERE online coupling was created, allowing the two models to exchange fields at each main physical time step (i.e a few minutes), thus enabling the possibility of the aerosol effects modelling.

This paper aims at presenting the online coupling developments made within the CHIMERE model along with an evaluation study of the aerosol–radiation interactions using the WRF-CHIMERE online coupling. Section 2 focuses on the CHIMERE-OASIS interface that was developed within the CHIMERE model along with the scheduling of the WRF-CHIMERE OASIS exchange operations. An evaluation test case along with model configurations are presented in Sect. 3. In Sect. 4, the computational performances of the WRF-CHIMERE online coupling are compared to the performances of both offline models. In addition, an estimation of the OASIS exchange burden is made. Case study simulations over the summer of 2012 are evaluated in Sect. 5. WRF and CHIMERE offline simulations are compared to two WRF-CHIMERE online simulations. In the first online simulation, the CHIMERE model is forced by the WRF model, without any feedback but at a higher rate than what is possible in offline mode. In the second online simulation aerosol optical properties are transferred from CHIMERE to WRF in order to take into account the aerosol–radiation interactions. Simulated results are compared to temperatures, AOD and concentration measurements. Note that applications presented in this paper focus on the aerosol–radiation interactions only. The study of cloud–aerosol interactions is currently ongoing and shall be the focus of a forthcoming paper.

2 Development of the WRF-CHIMERE coupled version

The CHIMERE2016a release included preliminary technical changes for the development of an online-coupled version of CHIMERE. CHIMERE preprocessors (for the calculation of emissions in particular) were included in its core. Indeed, in the case of an online simulation not all input data are known, prior to the simulation, for the entire simulation period. In particular, in the case of a WRF-CHIMERE online coupling, meteorological fields are received at each time step of a simulation, thus preventing the precomputation of meteorology-dependent variables such as mineral dust emission or biogenic emission fluxes. Furthermore, CHIMERE held a master–worker pattern where the master process performed all input/output operations. A more efficient pattern was implemented in which each worker performs parallel input/output operations, using the parallel-netcdf library (Li et al., 2003), without any master process.

Pursuing the development of an online version of CHIMERE in order to perform a WRF-CHIMERE coupling, more developments were made since the CHIMERE2016a release. These developments are described in Sects. 2.1 to 2.4 and fulfil the implementation of an online-coupled version of CHIMERE.

2.1 The CHISIS interface module

A Fortran module called CHISIS (CHImere/oaSIS) that interfaces CHIMERE and OASIS was developed. This module gathers all calls to OASIS subroutines required by CHIMERE in order to exchange fields with another model. Furthermore, a reading routine of the OASIS configuration file (i.e. the namcouple file) was included, thus allowing each model to be aware of coupling parameters (e.g. exchanged variable names, time steps, partitions, grids, models involved), leading to generic subroutines without any hard-coded information. Even though the CHISIS module was designed for CHIMERE, it does not contain any CHIMERE-specific material; therefore, it may be used in other models.

An OASIS interface module already exists within WRF as a WRF-NEMO coupling has already been implemented. However, WRF-NEMO exchanged variables were hard-coded within this interface module, making it difficult to reuse this module for the WRF-CHIMERE coupling. Thus, new compilation flags were added within the WRF code ("cpl_wrf_chimere" and "cpl_wrf_chimere") in order to distinguish the generic OASIS interface material that may be of use in a coupling with any model from the specific material of either WRF-NEMO or WRF-CHIMERE coupling.

2.2 OASIS configuration

The latest OASIS release, OASIS3-MCT, internally uses the Model Coupling Toolkit (MCT), developed by the Argonne National Laboratory in the USA, for parallel regridding and parallel distributed exchanges of the coupling fields (Larson et al., 2005; Jacob et al., 2005). To perform a WRF-CHIMERE coupling, the exchange of three-dimensional fields is required (e.g. temperature, wind velocity, pressure). A previous OASIS release, OASIS4, allows one to exchange three-dimensional variables (Redler et al., 2010); however, its code was too complex to evolve easily. Thus, OASIS developers decided to take a step back and use MCT with the OASIS3 release, which does not include the possibility of three-dimensional variable exchange. Therefore, three-dimensional spatial interpolation between model grids is not possible either. To overcome this issue, three-dimensional variables are decomposed into one-dimensional arrays prior to the exchange. Doing so makes it impossible for OASIS to perform a spatial interpolation between both model grids, as OASIS then considers one-dimensional unstructured arrays instead of spatial grids. Thus, both the WRF and CHIMERE models need to be run on the same horizontal grid in online mode. The WRF vertical grid may be used as it is not dependent on the sub-domain decomposition of each model.

Both the WRF and CHIMERE codes are parallelised using a decomposition into sub-domains which may be different for both models. An OASIS partition is required to describe each point of each sub-domain of each model within the same global index space. The OASIS "points" partition was chosen as it allows one to index each grid point separately, thus ensuring the preservation of the model's sub-domain decomposition flexibility (i.e. as is the case in offline mode), unlike other partitions that require one to index segments of points or rectangular regions of a domain.

2.3 OASIS exchange

2.3.1 Exchange from WRF to CHIMERE

In order to be run in offline mode, the CHIMERE model requires 28 meteorological variables at an hourly rate. In the offline version, these variables are read from WRF output files and include both two-dimensional variables (e.g. 10 m wind velocities, surface pressure, 2 m air temperature) and three-dimensional variables (e.g. base state pressure, cloud water mixing ratio, water vapour mixing ratio). CHIMERE performs a temporal interpolation between two sets of hourly WRF fields in order to compute species concentrations at every physical time step (i.e. a few minutes).

The WRF-CHIMERE online coupling enables the possibility of avoiding these sub-hourly temporal interpolations. Indeed, even though WRF output files may be hourly, WRF computes meteorology with a finer time step that is defined in its configuration file. Therefore, in online mode, the CHIMERE physical time step and the OASIS exchange frequency for meteorological fields are set to the same value. Hence, CHIMERE may receive fields at a sufficient rate to

avoid the need for a temporal interpolation of meteorological fields. The first version of the WRF-CHIMERE online coupling includes the exchange of the 28 WRF meteorological fields from WRF to CHIMERE through the OASIS coupler. Even though there is no feedback (i.e. exchange from CHIMERE to WRF), the use of instant WRF fields instead of interpolated fields will have an impact on the simulated results (see Sect. 5).

2.3.2 Aerosol optical properties feedback

The second version of the WRF-CHIMERE online coupling includes an aerosol optical properties feedback in order to take into account the aerosol–radiation interactions. The feedback consists of 23 three-dimensional variables, which are the single scattering albedos (SSAs) and the asymmetry factors (AFs) at 400 and 600 nm along with the AOD at 300, 400, 999 nm and at 16 long wavelengths ranging from 3400 to 55 600 nm.

Short-wave aerosol optical properties are already calculated within CHIMERE using the Fast-JX model for radiative transfer and online calculation of photo-chemical rates (Wild et al., 2000; Bian and Prather, 2002). The computation of long-wave parameters is done following the same method, by extending the radiative properties calculations within CHIMERE to the required long wavelengths.

Aerosol optical properties computed by CHIMERE from aerosol species are interpolated over the WRF vertical grid before being sent through the OASIS coupler. If the CHIMERE top level is lower than the WRF top level, the optical properties climatology from Péré et al. (2014) is used for short-wave aerosol optical properties, for the highest vertical levels. Long-wave aerosol optical properties of the highest vertical levels are set to zero above the CHIMERE top level.

Within the WRF model, short-wave AODs are interpolated over the required wavelengths using an Ångström power law, while the SSA and AF at 440 and 600 nm are interpolated assuming a linear relation. The long-wavelength AOD is added to the gas optical depth. Aerosol optical properties are used within the WRF model as inputs for the RRTMG (Rapid Radiative Transfer Model for General circulation models) scheme (Iacono et al., 2008).

2.3.3 Exchanges from CHIMERE to WRF

Aerosol optical properties are sent from CHIMERE to WRF through the OASIS coupler. The WRF "radt" parameter sets the frequency at which the RRTMG scheme is called within the WRF model. The recommendation from the WRF user's guide is to set the "radt" parameter to 1 min per kilometer of the grid distance between each grid cell (http://www2.mmm.ucar.edu/wrf/users/docs/user_guide_V3/ARWUsersGuideV3.pdf). As this frequency may be different from the OASIS exchange frequency for meteorological fields, "radt" is fixed to a multiple of this OASIS exchange frequency. Therefore, whenever WRF requires the aerosol optical properties, CHIMERE is able to send it. Regardless of the exchange frequency value, both WRF and CHIMERE may perform sub-iterations to ensure that the Courant–Friedrichs–Lewy condition is satisfied (see Fig. 1).

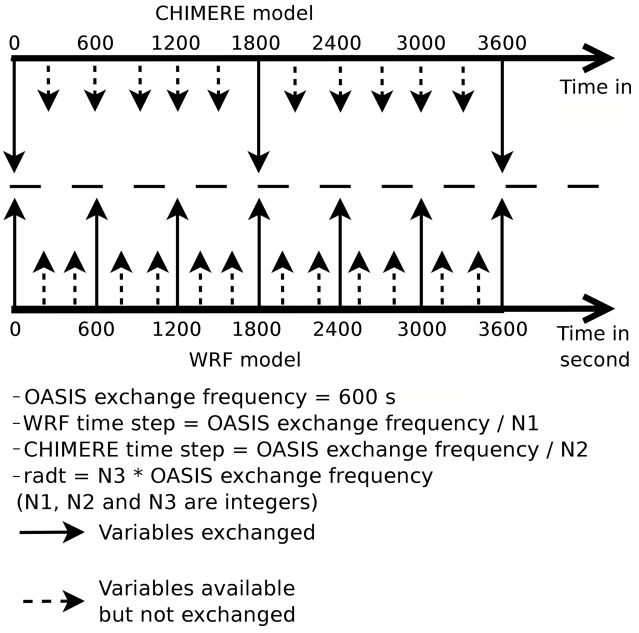

Figure 1. Illustration of variable exchange frequencies. The CHIMERE model receives WRF meteorological fields and sends the aerosol optical properties. The WRF model receives the aerosol optical properties and sends the meteorological fields. The OASIS exchange frequency defines both the frequency at which meteorological fields are exchanged (fixed here at 600 s) and the frequency at which aerosol optical properties are exchanged (fixed here at 1800 s, with N3 = 3). Both models may perform sub-iterations (here N1 = 3 and N2 = 2), in which case the previously received data are used during the sub-iterations. Note that the OASIS exchange frequency along with the N1, N2 and N3 integers are parameters that may be set by users.

2.4 Operations scheduling

In the case of a WRF-CHIMERE online-coupled simulation without any feedback, OASIS exchanges are made in one direction only (i.e. from WRF to CHIMERE). The operations scheduling is similar to what is done in offline mode, as CHIMERE is forced by WRF meteorological fields, but with a higher frequency. The initial meteorological fields sent are the WRF initial conditions. In Fig. 2 the WRF model runs faster than the CHIMERE model, leading to an accumulated delay between OASIS subsequent send and receive operations. However, as OASIS send operations are non-blocking, the WRF model may continue its calculations without having to wait for OASIS receive instructions within the CHIMERE model. In the case of a CHIMERE model that would run

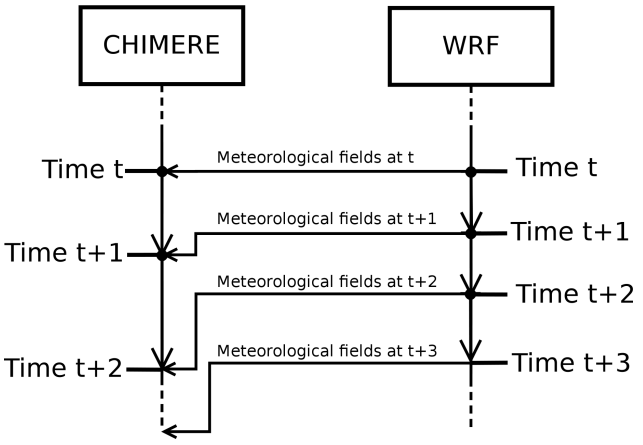

Figure 2. Operations scheduling in a WRF-CHIMERE online simulation with OASIS exchange from WRF to CHIMERE only.

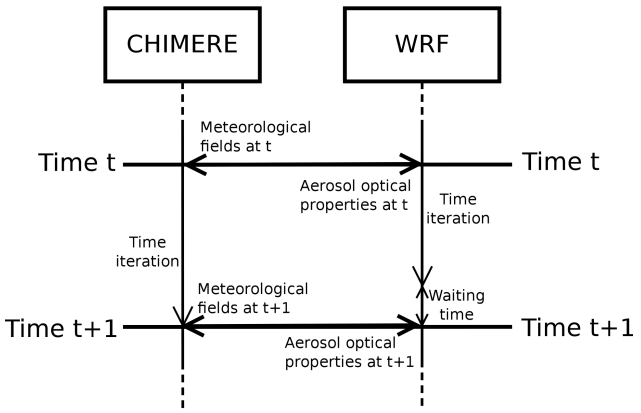

Figure 3. Operations scheduling in a WRF-CHIMERE simulation with the aerosol optical properties feedback.

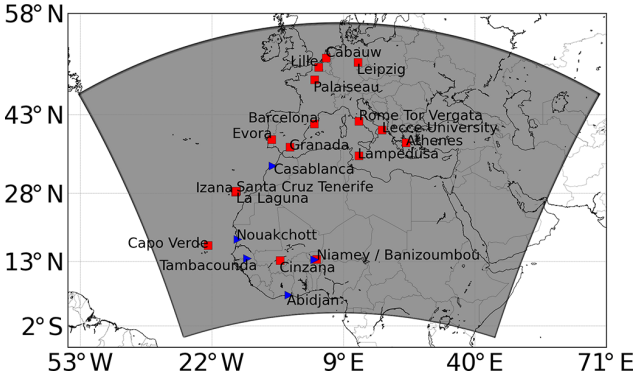

Figure 4. Simulated domain used in Sects. 4 and 5. AERONET stations are depicted with red squares and temperature atmospheric sounding stations with blue triangles.

faster than the WRF model, the CHIMERE model would wait for WRF meteorological fields.

In the case of two-way exchanges, the aerosol optical properties exchanges are performed right after the meteorological fields exchanges (i.e. at the beginning of each model time iteration). This allows the two models to perform their time iterations concurrently, thereby optimizing the overall computational burden (Fig. 3). Initial aerosol optical properties that are sent to WRF may be provided as an input file in CHIMERE, if available, or are set to zero otherwise. When the aerosol optical properties feedback is activated, the two models may need to wait for each other in order to receive the required fields that will allow them to continue the run. In any case, the overall WRF-CHIMERE online simulation time is expected to be close to the maximum of both WRF and CHIMERE offline run times.

Furthermore, in offline mode CHIMERE reads WRF meteorology files every hour, while in online mode it may receive WRF meteorology data at a higher rate. Therefore, in online mode CHIMERE needs to perform additional calls to WRF meteorology processing routines. In case aerosol optical properties are exchanged, calls to optical properties computation routines are also required. Thus, an increase in the computational time is expected within the CHIMERE model due to these additional operations.

3 Test case presentation

In order to evaluate both the computational burden and the model performances, three simulation types are defined.

- Offline: both WRF and CHIMERE are run sequentially. CHIMERE reads meteorological fields at an hourly rate from the WRF output file and the aerosol optical properties are not exchanged.
- Online case 1: WRF and CHIMERE are run online. Meteorological fields are sent through the OASIS coupler with a high temporal resolution (from WRF to CHIMERE). The aerosol optical properties feedback is not exchanged.
- Online case 2: WRF and CHIMERE are run online. Meteorological fields with a high temporal resolution (from WRF to CHIMERE) along with the aerosol optical properties (from CHIMERE to WRF) are sent through the OASIS coupler.

The simulated domain horizontal grid was built with a Lambert projection and has 159×109 points in longitude and latitude. It covers Europe, northern Africa, the Middle East and western Asia with a 60 km resolution (Fig. 4).

Both offline and online simulations are run with the same configuration. Note that both the WRF and CHIMERE versions that are used to perform all simulations presented in this paper are modified versions of the WRF 3.7.1 and CHIMERE2016a releases. These versions may be run in either offline or online mode and modifications from the

releases include exclusively the online modelling developments described in Sect. 2. Both WRF and CHIMERE configurations are presented in Sect. 3.1 and Sect. 3.2, respectively.

3.1 WRF model configuration

The WRF model is used in its non-hydrostatic configuration (Skamarock et al., 2007) and forced every 3 h by the meteorological analysis data of NCEP/GFS (Kalnay et al., 1996) provided on a regular $1.125° \times 1.125°$ grid. The model is run with 32 vertical levels, from the surface to 20 hPa, and with a 150 s integration time step. The RRTMG scheme, mandatory for the aerosol optical properties feedback, is used for both long- and short-wave radiations along with the Morrison two-moment microphysics scheme (Morrison et al., 2009). The surface layer scheme is the MM5 similarity theory scheme (Beljaars, 1995) and the surface physics scheme is the unified Noah land-surface model (Tewari et al., 2004). The Mellor–Yamada–Nakanishi–Niino (MYNN) planetary boundary layer's surface layer scheme (Nakanishi and Niino, 2006, 2009) is used and the cumulus parameterisation is based on the Grell–Freitas scheme (Grell and Freitas, 2014).

3.2 CHIMERE model configuration

The CHIMERE model takes into account four types of emission. Anthropogenic emission fluxes are pre-calculated fields from the HTAP 2010 inventory (Hemispheric Transport of Air Pollution), prepared by the EDGAR team (http://edgar.jrc.ec.europa.eu/national_reported_data/htap.php). Both biogenic and mineral dust emission fluxes are computed within the CHIMERE model using the MEGAN emissions scheme (Guenther et al., 2006) for the biogenic emissions and the dust production model described in Menut et al. (2015) for the mineral dust emissions. Finally, emissions related to biomass burning are pre-calculated using the model described in Turquety et al. (2014). The LMDZ-INCA global model climatology (Folberth et al., 2006) is used for aerosol and gas boundary conditions, while the GOCART model is used for mineral dust boundary conditions (Ginoux et al., 2001). The MELCHIOR2 chemical mechanism and the Bessagnet et al. (2004) aerosol module are used. The Fast-JX module, version 7.0b (Wild et al., 2000; Bian and Prather, 2002), was included in the CHIMERE model in order to compute photolysis rates along with aerosol optical depth (Mailler et al., 2016a). Dry and wet depositions are treated as described in Wesely (1989) and Loosmore and Cederwall (2004); 20 pressure-dependent vertical levels are used, from the surface up to 200 hPa. The WRF model fields computed on 32 σ levels, which are either received via the OASIS coupler (online mode) or read from the WRF output files (offline mode), are linearly interpolated over the 20 CHIMERE vertical levels.

Rea et al. (2015) studied the contribution of the different aerosol sources to surface particulate matter (PM), using the CHIMERE model with a similar configuration and over a similar domain during the summer of 2012. Results showed that both mineral dust and anthropogenic sources are the main contributors of PM over Europe and the Mediterranean region. Daily exceedances of the PM_{10} European Union limit ($50\,\mu g\,m^{-3}$) are captured at the right time. However, the number of exceedances is generally overestimated by the model, particularly in the northern part of the domain.

4 WRF-CHIMERE computational performances

WRF and CHIMERE offline simulation times along with WRF-CHIMERE online simulation times are compared in this section. Tests consist of 24 h simulations that are run on a 64-core server using the simulation domain and model configurations presented in Sect. 3. The exchange frequency is set to 15 min for both ways' exchanges; therefore, a total of 96 exchange time steps is performed. Several test simulations are run with different numbers of cores, which are equally distributed between WRF and CHIMERE models.

Considering the size of the domain and the variable's dimensions, the total number of exchanged points per iteration is over 6.4 million for WRF-to-CHIMERE exchanges. When adding the aerosol optical properties feedback it leads to a total of 19.2 million exchanged points per time iteration between the two models for both ways of exchanges. An estimation of the computational burden of these variable exchanges is made in Sect. 4.1, calculation and waiting times are studied using the LUCIA utility (Load-balancing Utility and Coupling Implementation Appraisal) that is distributed together with OASIS (Maisonnave and Caubel, 2014), in Sect. 4.2, and the load balance of each model is discussed in Sect. 4.3.

4.1 Comparison of both offline and online simulation times

The total online simulation durations are compared here to the offline simulation times. Time measurements were made using the Linux command "time". There is an uncertainty regarding these measurements that is not fully known, as it depends on the load of the computer that is used, which may vary during the simulations. However, simulations are long enough for the average times per iteration along with the trend to be significant.

Average simulation times per iteration are shown in Fig. 5 as a function of the number of cores per model. As the WRF model is much faster than the CHIMERE model, the maximum of both WRF and CHIMERE offline run times is equal to the CHIMERE offline run time. As expected, the CHIMERE model parallelisation induces a decrease in the overall computational time with the increase in the number of

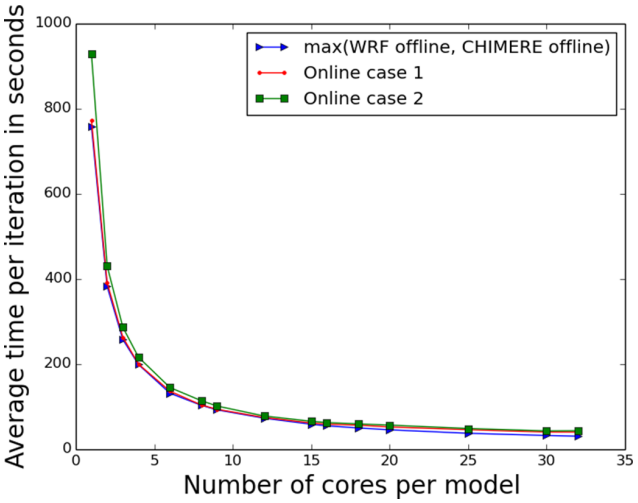

Figure 5. Evolution of the computational time per iteration as a function of the number of cores per model. Online case 1 refers to the online simulation without the aerosol optical properties feedback and online case 2 refers to the online simulation with the aerosol optical properties feedback.

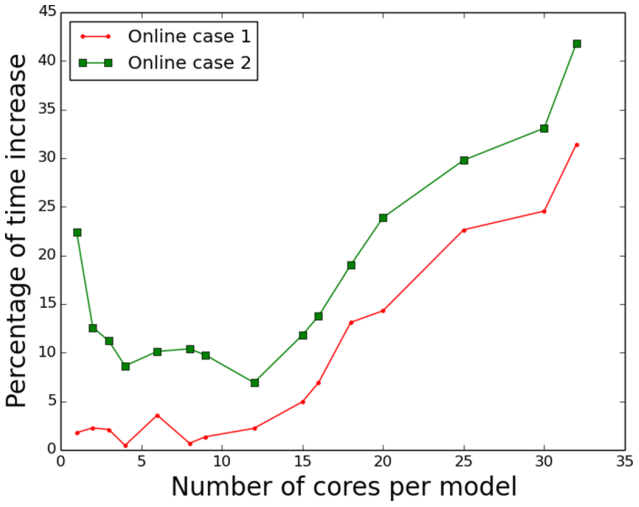

Figure 6. Evolution of the time increase from the offline simulation of both online simulations, as a function of the number of cores per model. Online case 1 refers to the online simulation without the aerosol optical properties feedback and online case 2 refers to the online simulation with the aerosol optical properties feedback.

cores. The decrease tendency is preserved in both online simulations; however, both online cases require more computational resources. The time increase is higher for online case 2 simulation than for online case 1 simulation, as more variables are exchanged and more computations are made (see Sect. 2.3). The highest time increase occurs when a lower number of cores is used (an up to 170 s increase using one core per model in the case 2 simulation). On the other hand, the percentage of the time increase from the offline simulation increases with the number of cores and reaches a 42 % increase when using 32 cores per model in the case 2 simulation (Fig. 6). A gradual increase is observed when more than 12 cores per model are used. Indeed, the additional burden due to the coupling does not decrease as steadily as the offline CHIMERE model burden, when increasing the number of cores. Part of the additional burden may be attributed to the OASIS exchange along with the variable formatting routines. The other part is related to additional calls to some CHIMERE routines that are made in online mode (i.e. a more frequent meteorology treatment subroutine in case 1 along with optical properties computations in case 2). A measure of the computational burden that may be attributed to variable exchange subroutines has been made using the "cpu_time" Fortran routine. These subroutines are responsible for less than 3 % of the time increase for both online cases when using 32 cores per model. Therefore the increase in the computational burden that may be attributed to the OASIS exchange is not significant compared to the model computations.

4.2 Calculation and waiting times

Results presented in this section were obtained using the LUCIA utility on the 32 cores per model simulations, which provide the total calculation and waiting times for both models and for both the case 1 and case 2 simulations. Online case 1 results indicate that WRF performs fewer calculations than CHIMERE, i.e. 770 s for WRF vs. 3630 s for CHIMERE. This is consistent with the fact that there is almost no waiting time for the CHIMERE model (i.e. 10 s), as WRF meteorological fields are always available when CHIMERE required them. Even though OASIS send operations are non-blocking, the WRF model waits for CHIMERE for 2890 s. A possible explanation is that WRF is so far ahead of CHIMERE that its sending buffer is full. Thus, WRF needs to wait for CHIMERE receive instructions to empty its buffer and to continue the run. Nevertheless, as CHIMERE is computationally more costly, WRF waiting times do not induce any additional burden on the overall WRF-CHIMERE online simulation. Similar results are observed for the case 2 simulation. As both model iterations are done in parallel, the aerosol optical properties feedback does not induce a significant change in the overall balance between the two models.

4.3 Load balance of each model

Results show an imbalance in the load of the two models as in both online cases the WRF model performs fewer calculations than the CHIMERE model. As the load of each model may depend on criteria such as the selected options within both WRF and CHIMERE configuration files or the geometry of the domain, the ratio of cores that will optimise the

computational burden is not unique, and it would not be fair to give one specific ratio. Therefore, here, the same number of cores was attributed to both models. This is an arbitrary choice made in order not to favour either WRF or CHIMERE in the study. Ultimately, this choice needs to be revised using iterative methods to estimate the optimum ratio of the number of cores for each model. In our case, attributing a lower number of cores to WRF and a higher number of cores to CHIMERE will reduce the overall computational time. Based on the Sect. 4.2 results, using 4 or 5 times more cores with CHIMERE than with WRF may be an efficient ratio.

5 WRF-CHIMERE evaluation study during a mineral dust event

WRF-CHIMERE online simulations are confronted in this section with both measurements and a corresponding offline simulation. The simulated period starts on 15 May 2012 and ends on 14 July 2012, thereby covering the June 2012 mineral dust outbreak event (Nabat et al., 2015). Simulated results from 15 until 31 May are considered to be spin-up time. Thus only the simulated results from 1 June are considered for the evaluations made in the following sections. The OASIS exchange frequency for meteorological fields, thus the CHIMERE physical time step, is set to 15 min, and the WRF "radt" parameter is set to 30 min. WRF meteorological fields and CHIMERE output concentrations are stored every hour for the analysis.

Simulated radiation budgets, surface temperatures and wind velocities are compared in Sect. 5.1. Simulated results are then successively evaluated against University of Wyoming vertical temperature atmospheric soundings (Sect. 5.2), MODIS AOD (Sect. 5.3), AERONET AOD (Sect. 5.4) and AirBase PM_{10} concentration data (Sect. 5.5).

5.1 Feedback impact on radiation budget, surface temperatures and wind velocities

The radiative forcing is defined as the difference in the net radiation flux (down–up) between both online simulations. Changes in the radiation budget induced by the optical properties feedback are studied here through the radiative forcing induced by the aerosol optical properties feedback. Figure 7 shows difference maps between the two online cases of the average radiation budget at the ground surface for both long waves and short waves. Long-wave radiative forcing attributed to the optical properties feedback in the case 2 simulation is positive, up to $35\,W\,m^{-2}$, and is mainly located over desert areas (i.e. the Saharan region and the Arabian Peninsula). A negative forcing observed over the Atlantic Ocean is of lesser importance, less than $5\,W\,m^{-2}$. An opposite behaviour is obtained for short-wave radiation fluxes, as there is a negative forcing, up to $55\,W\,m^{-2}$ over the Saharan region and the Arabian Peninsula, and a positive forcing of a lesser importance over the Atlantic Ocean, less than $28\,W\,m^{-2}$. The average forcing over the simulated domain is a cooling of $4.8\,W\,m^{-2}$ (i.e. radiative forcing of $5.8\,W\,m^{-2}$ for long waves and $-10.7\,W\,m^{-2}$ for short waves).

The perturbation of the WRF radiative scheme outputs depends on the CHIMERE aerosol optical properties, and thus on the CHIMERE aerosol load. In our case the perturbation in the optical properties is dominated by mineral dust, as observed changes occur over regions where mineral dust constitutes the main aerosol type (i.e. the Saharan region and the Arabian Peninsula). Mineral dust emission fluxes computed by the CHIMERE during the online case 1 simulation model are shown in Fig. 8 in order to visualise the locations of the main mineral dust sources. Mineral dust both absorbs and scatters solar radiation, leading to both negative and positive radiative forcing, depending on the radiation wavelength and on the mineral dust size distribution (Sokolik and Toon, 1996). Aerosol absorption of solar radiation induces a heating of the atmosphere, and thus a reduction of the cloud coverage. This effect is referred to as the aerosol semi-direct effect (Hansen et al., 1997; Ramanathan et al., 2001) and is responsible for part of the changes in the radiative forcing. Off the western Saharan coast, high mineral dust concentrations cause a reduction of the cloud coverage, thereby inducing an increase in the short-wave radiative forcing in the online case 2 simulation.

In Guo and Yin (2015) the mineral dust impacts on the regional precipitation and summer circulation in eastern Asia are studied. A negative short-wave radiative forcing along with a positive long-wave radiative forcing induced by the presence of mineral dust particles are observed. The long-wave radiative forcing is less than $50\,W\,m^{-2}$ and the short-wave radiative forcing is less than $-70\,W\,m^{-2}$. Even though the simulated areas are different, the impacts of mineral dust on the radiative forcing are in accordance with the results presented in the current paper.

A direct consequence of the changes in the radiative forcing is a perturbation of the surface temperatures. Figure 9 maps show a moderate decrease in the surface temperatures (i.e. less than 0.4°) over Sub-Saharan Africa and Europe and over the northern part of the Atlantic Ocean, where the radiative forcing (short-wave + long-wave) is negative. Over the Saharan region, the Arabian Peninsula and off the western Saharan coast, temperatures increase, where the radiative forcing (short-wave + long-wave) is positive. The maximum increase is 2.6° over a grid cell located in north-eastern Niger.

Figure 10a presents a 4-day time series (1 to 4 June) of surface temperatures over the north-eastern Niger grid cell in which the maximum differences in average surface temperatures occur. The diurnal profile shows that an increase in temperatures occurs during nighttime (up to 5°), while a slight decrease in temperatures occurs during daytime (less than 1°). Figure 10b shows that the short-wave effect prevails during daytime, thus creating a decrease in the surface

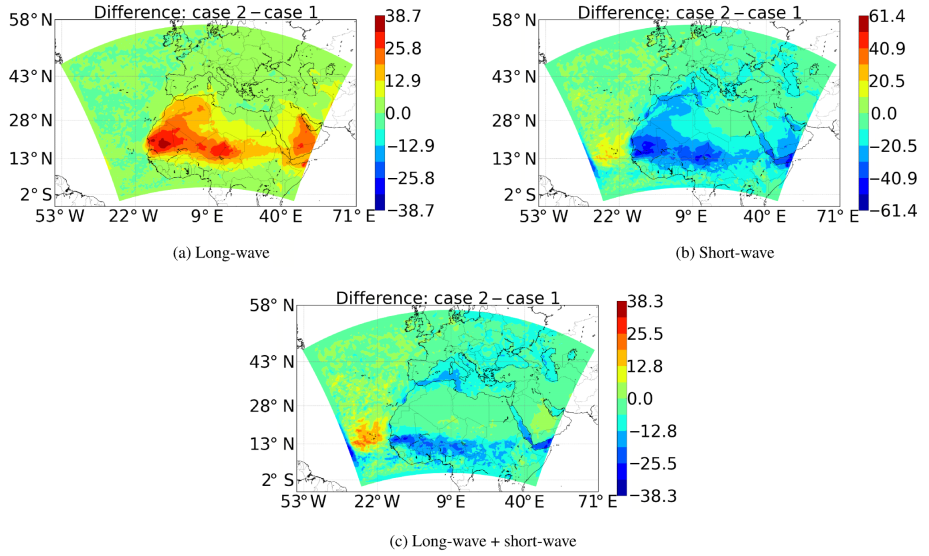

(a) Long-wave

(b) Short-wave

(c) Long-wave + short-wave

Figure 7. Difference in the WRF radiation budget at the ground surface between both online simulations (all-sky fluxes). Fluxes are in $\mathrm{W\,m^{-2}}$ and are averaged in time over the period ranging from 1 June to 14 July.

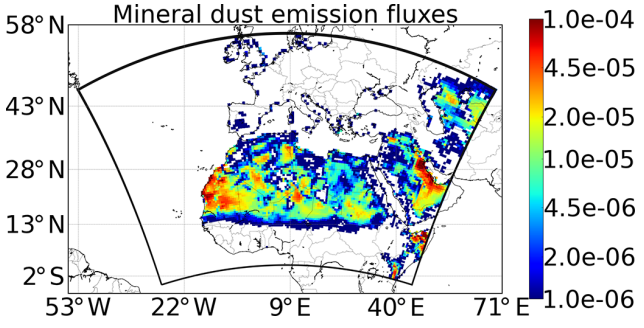

Figure 8. CHIMERE mineral dust emission fluxes (in $\mathrm{g\,m^{-2}\,s^{-1}}$) averaged over the period ranging from 1 June to 14 July (online case 1 simulation).

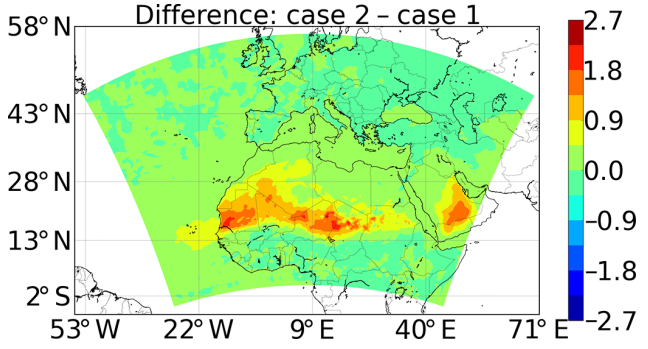

Figure 9. Difference map of WRF temperature at 2 m from the surface averaged over the simulated period ranging from 1 June to 14 July (in Kelvin).

temperatures, while the long-wave effect alone contributes at night due to the earth outgoing long-wave radiations, inducing an increase in the temperatures. This is also observed in Yue et al. (2010); Guo and Yin (2015).

Another consequence of the perturbation of the radiative forcing is the alteration of the wind velocities. Figure 11 shows that the use of the aerosol optical properties feedback in the online case 2 simulation induces both an increase (up to $0.5\,\mathrm{m\,s^{-1}}$) and a decrease (up to $0.4\,\mathrm{m\,s^{-1}}$) in the wind module over part of the Saharan region and the Arabian Peninsula. As the wind velocity is the main parameter influencing mineral dust emissions, changes in CHIMERE aerosol content are also observed. The perturbation in the mineral dust emission fluxes is sporadic, due to the non-linear property of mineral dust emissions, and is less than 0.1 % of the total mineral dust emission fluxes over the simulated domain.

5.2 Comparison with the University of Wyoming atmospheric sounding vertical temperature data

Atmospheric sounding temperature data were gathered at five stations over the Saharan region and the Arabian Peninsula (see Fig. 4 for station locations), from the University of Wyoming website (http://weather.uwyo.edu/upperair/sounding.html). Differences in temperature vertical profiles between sounding and online modelled values are displayed in Fig. 12 at selected times. Results are interpolated over the soundings' vertical levels. Stations are located in the western Sahara (Tambacounda, Abidjan, Nouakchott and Niamey), where the impact of mineral dust emissions, and thus the differences in solar radiation, are important. The profiles are shown for 23 June, during the end of June mineral dust outbreak (i.e. from 21 to 23 June). In addition, temperature vertical profiles are shown at the Casablanca station for both 23

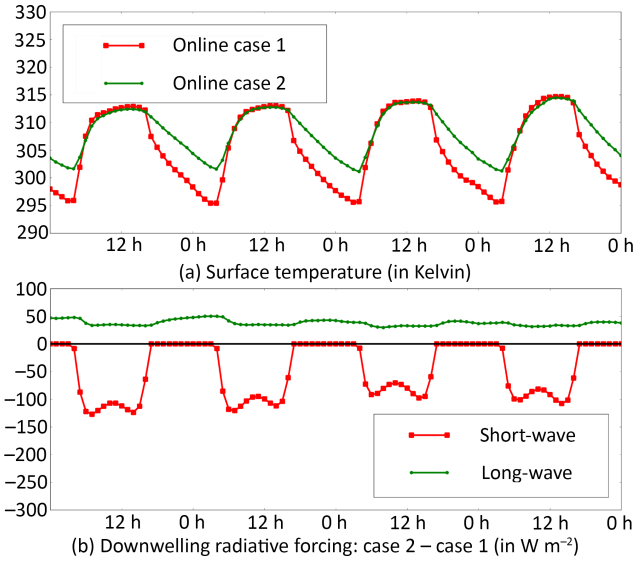

Figure 10. Surface temperature and downwelling radiative forcing 4-day time series (1 to 4 June) over a grid cell in north-eastern Niger (GMT time).

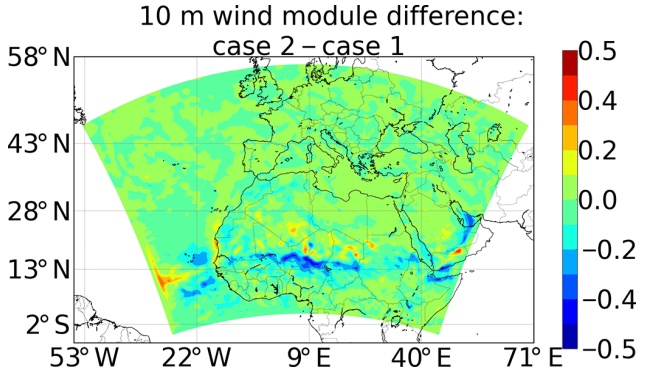

Figure 11. The 10 m high wind module difference map between online case 1 and case 2 (in $m\,s^{-1}$) averaged in time over the period ranging from 1 June to 14 July.

and 26 June. Therefore, the two profiles at the Casablanca station allow one to compare vertical temperature profiles with a low and high level of mineral dust.

Differences between observations and modelled values lie between −3.1° at the Tambacounda station and 6.5° at the Nouakchott station. Differences between modelled values are small at higher levels (roughly above 5000 m, where mineral dust concentrations are low) and are less than 0.12° at the highest level at all stations, except for Casablanca on 26 June, where the temperature difference between both online cases at the highest level is 0.5°. Therefore, only the lower part of the vertical profiles is shown in Fig. 12.

The online case 2 simulation yields the temperature generally closer to observations at altitudes of up to 1–2 km, compared to case 1. At Tambacounda, for instance, the case 2 simulation reduces the underestimation of measurements by 0.6°.

The differences are higher, however, at Nouakchott on 23 June and Casablanca on 26 June between 1.5 and 4.5 km. The atmospheric cooling with height is already overestimated within this layer in case 1, by up to −2.5°. This overestimation becomes slightly higher in case 2, with an additional 0.5°. The cooling overestimation can be related to excessive cloud formation in the WRF model in this region, which is reinforced through the aerosol–radiation interactions in case 2. In general, the impact of the aerosol optical properties feedback can lead to differences of up to 1.7°.

5.3 Comparison with MODIS AOD

The Moderate Resolution Imaging Spectroradiometer (MODIS) satellite data are compared to the modelled AOD (Levy et al., 2015). MODIS Dark-Target and Deep-Blue products at 550 nm are merged in order to form a single map. The Deep-Blue product is preferred when both products are available at a given point, as it is more accurate over desert areas (Hsu et al., 2013). Data are averaged over the period ranging from 1 June to 14 July. Modelled values were also averaged in time, using only modelled values at times at which a MODIS observation is available. As CHIMERE aerosol optical depth is calculated at fixed wavelengths (i.e. 200, 300, 400, 600 and 999 nm), the AOD is interpolated at 550 nm following an Ångström power law. The corresponding MODIS AOD map is displayed in the top left corner of Fig. 13 and the difference between MODIS and offline AOD is shown in the top right corner of Fig. 13. In addition, both online AODs are shown as the difference between modelled values rather than the difference with the MODIS AOD (bottom of Fig. 13).

Over major sources of mineral dust, such as the Saharan region and the Arabian Peninsula, the MODIS AOD values are high (up to 1.3). However, even higher values are observed over the eastern side of the Caspian Sea, the Red Sea and the Zagros Mountains (up to 3). Both offline and online simulations failed to detect these high values over those three regions. Such CHIMERE/MODIS AOD differences were already observed in Menut et al. (2015) and in Mailler et al. (2016a). Over the eastern part of the Caspian Sea, those differences may be attributed to missing mineral dust as it is an arid region. In Nabat et al. (2015) the MODIS data overestimate the MISR (Multiangle Imaging SpectroRadiometer Kahn et al., 2005) satellite product and AERUS-GEO (Aerosol and surface albedo Retrieval Using a directional Splitting method; application to GEO data by Carrer et al., 2014) over the Red Sea and on the eastern side of the Caspian Sea. This suggests that the high MODIS AOD values may be attributed to an overestimation made by the MODIS aerosol retrieval algorithm.

Over Europe, North Africa and the Atlantic Ocean, differences between MODIS and the offline simulated AOD are

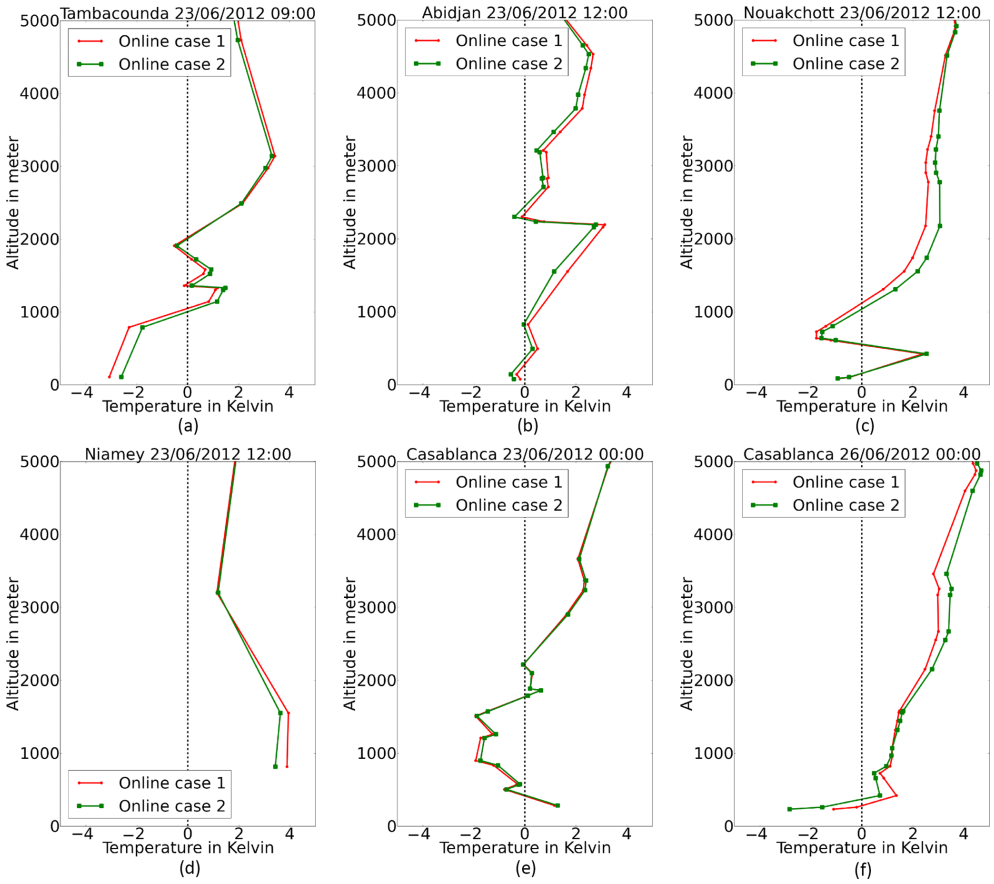

Figure 12. Difference in vertical profiles of temperature (modelled values−radiosounding values).

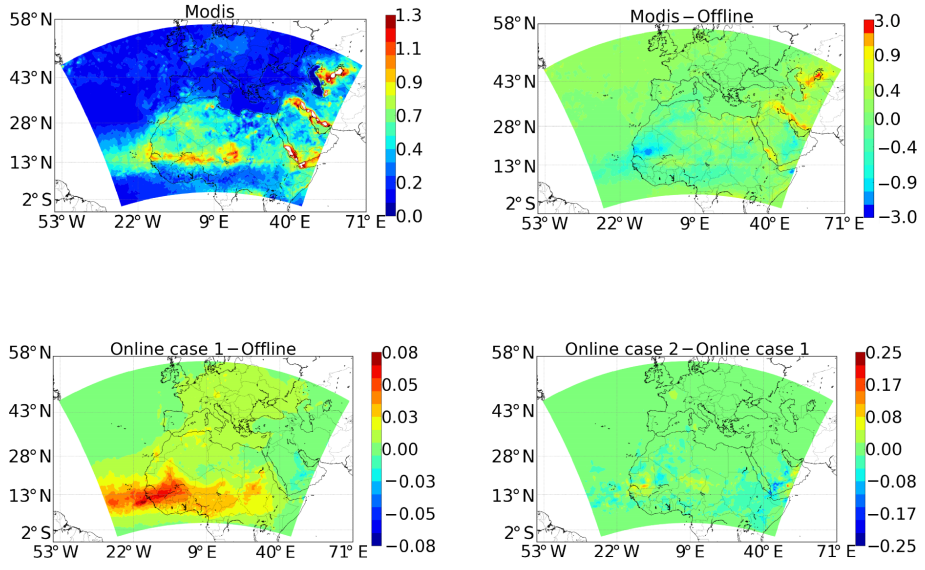

Figure 13. AOD and AOD difference maps at 550 nm, averaged in time over the period ranging from 1 June to 14 July.

Table 1. Performance indicators of WRF-CHIMERE modelled values against daily AERONET AOD measurements over the period ranging from 1 June to 14 July. Meas, Off, On1 and On2 correspond to measurements, offline simulation, online case 1 simulation and online case 2 simulation, respectively. *N* is the number of observations and RMSE is the root mean square error.

Station names	*N*	Mean values				RMSE			Correlation			Bias		
		Meas	Off	On1	On2	Off	On1	On2	Off	On1	On2	Off	On1	On2
Izana	44	0.12	0.28	0.29	0.29	0.25	0.26	0.24	0.94	0.94	0.95	0.16	0.17	0.16
Lampedusa	44	0.18	0.32	0.33	0.33	0.23	0.25	0.25	0.77	0.77	0.75	0.14	0.15	0.15
Granada	44	0.18	0.24	0.24	0.25	0.14	0.14	0.15	0.85	0.85	0.84	0.05	0.06	0.06
Lecce University	44	0.12	0.15	0.16	0.16	0.08	0.08	0.09	0.72	0.72	0.71	0.03	0.04	0.04
Santa Cruz Tenerife	42	0.26	0.3	0.31	0.3	0.21	0.21	0.2	0.86	0.87	0.89	0.03	0.04	0.04
Evora	42	0.11	0.12	0.13	0.13	0.09	0.1	0.1	0.95	0.95	0.94	0.02	0.02	0.02
Rome Tor Vergata	41	0.13	0.18	0.19	0.19	0.14	0.14	0.14	0.82	0.82	0.82	0.05	0.06	0.06
Banizoumbou	37	0.69	0.65	0.69	0.68	0.29	0.29	0.3	0.44	0.41	0.37	−0.04	0.0	−0.01
Cinzana	35	0.7	0.62	0.68	0.68	0.45	0.45	0.45	0.29	0.25	0.23	−0.08	−0.02	−0.02
Capo Verde	31	0.53	0.87	0.91	0.88	0.53	0.55	0.51	0.47	0.48	0.51	0.35	0.38	0.36
La Laguna	31	0.29	0.34	0.35	0.34	0.2	0.2	0.18	0.89	0.89	0.91	0.05	0.06	0.06
Athenes	30	0.11	0.14	0.14	0.14	0.05	0.06	0.06	0.74	0.74	0.72	0.02	0.03	0.03
Leipzig	27	0.11	0.11	0.13	0.12	0.11	0.12	0.11	0.5	0.5	0.5	0.0	0.01	0.01
Cabauw	23	0.12	0.06	0.06	0.06	0.09	0.08	0.08	0.2	0.19	0.19	−0.06	−0.06	−0.06
Palaiseau	22	0.11	0.07	0.08	0.08	0.08	0.07	0.08	0.67	0.67	0.67	−0.04	−0.03	−0.03
Lille	21	0.1	0.07	0.07	0.07	0.09	0.09	0.09	0.48	0.48	0.48	−0.03	−0.03	−0.03
Barcelona	20	0.2	0.23	0.25	0.24	0.17	0.18	0.19	0.8	0.8	0.77	0.03	0.04	0.04

less than 0.4. Major differences occur in the western part of the Sahara (south of Mauritania) and in the southern part of the Arabian Peninsula, where the CHIMERE model overestimates the MODIS AOD by up to 1.4. Differences are most likely due to an overestimation of mineral dust emissions, which are the main AOD contributors in those areas.

The more resolved meteorology in online case 1 simulation mainly induces higher AOD than the offline simulation. The AOD increase ranges from 0.03 over Europe up to 0.08 over southern Mauritania and western Mali. Changes induced by the aerosol optical properties feedback are more important (difference of up to 0.25); however, it induces both increases and decreases, principally over both Africa and the Arabian Peninsula. Differences may be explained by the alteration of the wind velocities in these areas, thus inducing alterations of the mineral dust emissions, as the wind velocity is the main parameter influencing mineral dust production (Fig. 11).

5.4 Comparison with AERONET AOD

Daily AOD at 675 nm of both level 2.0 quality assured AERONET data (Holben et al., 1998) and CHIMERE AOD are compared in this section. The locations of AERONET stations are shown in Fig. 4.

A mineral dust outbreak occurred over western Africa between 21 and 23 June (Nabat et al., 2015). Due to a lack of data during this period, this mineral dust outbreak is not visible in the AOD time series at the Capo Verde and Cinzana stations. However, particles have been transported along the African coast up to southern Spain; therefore, it is visible in the AOD time series at the Izana, La Laguna, Santa Cruz Tenerife (24 to 30 June), Granada (24 to 30 June), Evora (25 to 29 June) and Barcelona (27 June to 1 July) stations (Fig. 14). Even though AOD peak intensities tend to be overestimated, models manage to predict efficiently the times at which high AOD events occur. Although high AOD events are detected at the same moment in each simulation, variations in the peak intensities appear. However, time series alone are not sufficient to infer whether or not one simulation performs better than another because the three simulation results are close to each other.

AOD performance indicators over the period ranging from 1 June to 14 July are shown in Table 1 and are defined as

- correlation,

$$\frac{\sum_{i=1}^{N}(O_i-\overline{O})(M_i-\overline{M})}{\sqrt{\sum_{i=1}^{N}(O_i-\overline{O})^2}\sqrt{\sum_{i=1}^{N}(M_i-\overline{M})^2}},$$

- RMSE (root mean square error),

$$\sqrt{\frac{1}{N}\sum_{i=1}^{N}(M_i-O_i)^2},$$

- bias,

$$\frac{1}{N}\sum_{i=1}^{N}(M_i-O_i),$$

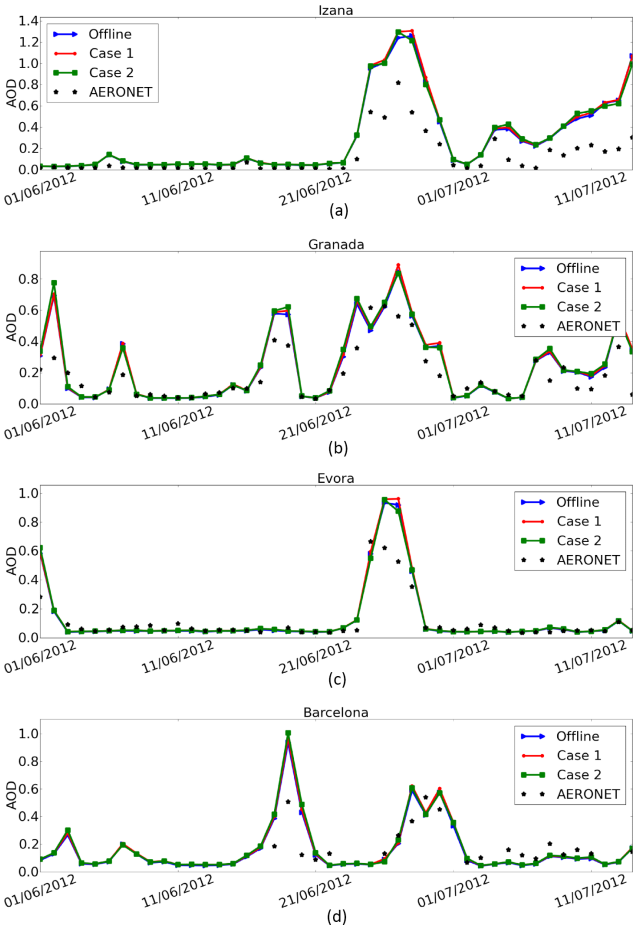

Figure 14. AERONET and modelled AOD time series.

where M_i and O_i are the modelled and observed values, respectively, and $\overline{x} = \frac{1}{N}\sum_{i=1}^{N} x_i$.

Apart from the Lampedusa station, RMSE is less than 0.19 at all European stations, while at African stations it ranges from 0.18 in La Laguna up to 0.55 in Capo Verde. Six stations have a particularly low correlation (less than 0.5), Cabauw (0.19 to 0.2), Cinzana (0.23 to 0.29), Banizoumbou (0.37 to 0.44), Lille (0.48), Capo Verde (0.47 to 0.51) and Leipzig (0.5), while correlations at other stations are higher, ranging from 0.67 at Palaiseau up to 0.95 at Evora and Izana. Bias is higher at the Izana, Capo Verde and Lampedusa stations (from 0.14 to 0.38) and is less than 0.08 elsewhere. The three African stations located near major mineral dust sources (i.e. Banizoumbou, Cinzana and Capo Verde) present lower performances. This may be explained by the difficulty in reproducing mineral dust events within the model, as mineral dust is the main AOD contributor at these stations. If a mineral dust event is not detected or if it is wrongly detected by the model, the impact on the AOD may be important.

Models overestimate measurements at 12 out of 17 stations. Furthermore, average AOD is higher in both online simulations than with the offline simulation. The offline simulation performs equivalently or better at European stations (higher correlation and lower RMSE and bias); however, simulated results are close to each other. Differences between modelled values are higher at African stations (mean value differences of up to 0.6) than at European stations (mean value differences of up to 0.2 at the Barcelona station). The online case 2 has higher correlations (up to 0.4 higher) and a lower RMSE (up to 0.2 lower) at the Izana, Santa Cruz Tenerife, Capo Verde and La Laguna stations than the other simulations. At both the Banizoumbou and Cinzana stations the offline simulation presents higher correlations and lower negative biases than the online simulations.

5.5 Comparison with AirBase PM_{10} concentrations

Hourly PM_{10} measurement from the European Air quality dataBase (AirBase) of the European Environment Agency (http://acm.eionet.europa.eu/databases/airbase) are used in this section for comparison with CHIMERE PM_{10} concentrations. As in Rea et al. (2015), only rural and background stations are considered for the comparison in order to avoid sites which are strongly influenced by local sources. In addition, stations with a minimum of 300 measurements during the period ranging from 1 June to 14 July are selected, leading to a total of more than 940 remaining stations located over Europe.

Averaged performance indicators show that all simulations overestimate measurements and that the overestimation is higher with both online simulations ($6.8\,\mu g\,m^{-3}$) than with the offline simulation ($1.7\,\mu g\,m^{-3}$). Correlations are lower (differences of up to 0.17) and the RMSE is higher (differences of up to $22\,\mu g\,m^{-3}$) at most stations for both online simulations. The increase in PM_{10} concentrations in online simulations is consistent with the results of Sect. 5.3 and 5.4, in which the more resolved meteorology in the online case 1 simulation induces higher AOD over Europe. Indeed, higher-frequency meteorological fields, received by CHIMERE from WRF, in the online simulations are associated with higher temporal variability, which are smoothed out through the temporal interpolation in the offline simulation. In the case of the wind velocity for instance it can lead to higher mineral dust emissions, which is a threshold process, and/or particulate matter resuspension, thus increasing the PM_{10} concentrations in online mode. A deeper analysis is needed, using PM_{10} concentration measurements over Africa, in order to assess the overall impact of the WRF-CHIMERE coupling on PM_{10} concentrations.

6 Discussion and conclusions

An online coupling between the WRF and CHIMERE models through the OASIS coupler has been developed. WRF meteorological fields along with CHIMERE aerosol optical

properties are exchanged in order to simulate the aerosol–radiation interactions.

The WRF-CHIMERE online model requires more computational resources than the offline models, mainly due to the CHIMERE model, as the WRF model is less demanding. The computational time increase within the online model is mostly related to additional calls to the routines added to prepare the fields before being sent through the coupler and to process the received fields. On the other hand, the increase in computational time related to OASIS exchanges is not significant. Therefore, increasing the amount of OASIS exchange in future development would not be an issue.

Both offline and online simulations of 2 months of the summer of 2012 are compared. The use of the optical properties feedback induces a $5.8\,\mathrm{W\,m^{-2}}$ average increase in long-wave radiative forcing and a $10.7\,\mathrm{W\,m^{-2}}$ decrease in short-wave radiative forcing. Consequences of the radiative forcing perturbation are changes in the averaged surface temperatures (i.e. an increase of up to 2.6° over desert areas and a moderate decrease of less then 0.4° elsewhere) and wind velocities (i.e. averaged differences ranging from -0.4 to $0.5\,\mathrm{m\,s^{-1}}$). Diurnal profiles over the grid cell where the average temperature difference is maximum show that temperatures decrease slightly during daytime, when the short-wave effect prevails. On the other hand, temperatures increase at night, when the long-wave effect alone contributes due to the earth outgoing long-wave radiations. Therefore, the modelling of the aerosol–radiation interactions, through the aerosol optical properties feedback, is not negligible. Observed AOD by the AERONET network is compared to modelled AOD, leading to higher correlations and lower RMSE at African stations when using the aerosol optical properties feedback while simulating a dust event. Over Europe, differences between simulations are of minor importance.

The aerosol–radiation coupling is found to better simulate the temperature in the lower layer of the atmosphere (1 to 2 km). At the same time it can amplify the overestimation of the cooling in the middle troposphere, through the aerosol–radiation interactions. Specific studies are needed, beyond the scope of this model presentation article, in order to evaluate these effects using more available data on the atmospheric vertical structure.

The evaluations of the AQMEII project (Im et al., 2015a) performed 10 online- and 1 offline-coupled model simulation for Europe and have not clearly concluded on the impact of the online coupling on aerosol simulation performance. The offline model (BG2) showed the highest AOD555 over Europe (their Fig. 13c), but the differences between the online-coupled models, attributed to their parameterisations, emission and boundary condition treatment, appear to be similar to the difference between their median and the offline-coupled simulation. As for the PM_{10} and $PM_{2.5}$, the offline simulation results have not shown any particular difference from the online simulations.

This is in agreement with the findings of the present study. Our results suggest that the online coupling between meteorology and aerosols, taking into account aerosol–radiation interactions, might be only beneficial for model performance for sufficiently large aerosol loads. Further evaluation studies are needed, relating the observed aerosol loads and their chemical compositions to the model performance improvements due to the meteorology–aerosol coupling.

Even though the radiative coupling between WRF and CHIMERE does not necessarily improve the model performances in terms of biases and correlations of PM_{10} aerosols in Europe, these results open the possibility of using the WRF-CHIMERE coupled system to simulate cases where the radiative effects of optically thick aerosol plumes on the atmosphere are significant, and to examine the impact of these dense plumes on meteorology and their feedbacks on the advected plumes themselves. Results presented in this paper emphasise that using the aerosol optical properties feedback induces non-negligible changes in model outputs. In addition, up to now emissions have been designed for offline models, and some modifications within emission parameterisations, mineral dust in particular, may be required in online mode. For instance, the more resolved meteorology in online simulation induces an increase in the wind velocity variability. A Weibull distribution is used to account for the wind variability within the mineral dust emission parameterisation (Cakmur et al., 2004), and its parameters might need to be adjusted to yield better model performance in the online-coupled case.

Online modelling developments presented in this paper will be made publicly available through a future CHIMERE release. The development of the WRF-CHIMERE online coupling continues with the implementation of another WRF-CHIMERE feedback, aiming at modelling the aerosol–cloud microphysical interactions. In addition, as the CHIMERE model is now interfaced with the OASIS coupler, future work may involved online coupling with other models.

7 Code availability

The WRF model is available at http://www.wrf-model.org/index.php (Skamarock et al., 2007) and OASIS coupler code is available at https://verc.enes.org/oasis (Valcke et al., 2015). The CHIMERE model is provided under the GNU General Public License and is available on the CHIMERE website: http://www.lmd.polytechnique.fr/chimere/ (Mailler et al., 2016b). Both WRF and CHIMERE online coupling developments will be made available in a future CHIMERE release and are available upon request.

Competing interests. The authors declare that they have no conflict of interest.

Acknowledgements. The authors acknowledge the French Direction Générale de l'Armement for funding the APPAD project, the COPERNICUS-DD program for funding the NATORGA project and the University of Geneva for its support. This work was also supported by the DRUMS (DeseRt dUst Modeling: performance and Sensitivity evaluation; project ANR-ASTRID-DRUMS-2012) research program funded by the ASTRID fund call of the French Agence Nationale de la Recherche (ANR). We thank the OASIS modeling team for their support with the OASIS coupler. Finally, we thank the National Aeronautics and Space Agency for the availability of the MODIS data, the investigators and staff who maintain and provide the AERONET data, the University of Wyoming for the availability of the atmospheric soundings, and the European Environment Agency for providing the AirBase data.

Edited by: G. A. Folberth
Reviewed by: two anonymous referees

References

Baklanov, A., Schlünzen, K., Suppan, P., Baldasano, J., Brunner, D., Aksoyoglu, S., Carmichael, G., Douros, J., Flemming, J., Forkel, R., Galmarini, S., Gauss, M., Grell, G., Hirtl, M., Joffre, S., Jorba, O., Kaas, E., Kaasik, M., Kallos, G., Kong, X., Korsholm, U., Kurganskiy, A., Kushta, J., Lohmann, U., Mahura, A., Manders-Groot, A., Maurizi, A., Moussiopoulos, N., Rao, S. T., Savage, N., Seigneur, C., Sokhi, R. S., Solazzo, E., Solomos, S., Sørensen, B., Tsegas, G., Vignati, E., Vogel, B., and Zhang, Y.: Online coupled regional meteorology chemistry models in Europe: current status and prospects, Atmos. Chem. Phys., 14, 317–398, doi:10.5194/acp-14-317-2014, 2014.

Beljaars, A. C. M.: The parametrization of surface fluxes in large-scale models under free convection, O. J. Roy. Meteorol. Soc., 121, 255–270, doi:10.1002/qj.49712152203, 1995.

Bessagnet, B., Hodzic, A., Vautard, R., Beekmann, M., Cheinet, S., Honoré, C., Liousse, C., and Rouil, L.: Aerosol modeling with CHIMERE – preliminary evaluation at the continental scale, Atmos. Environ., 38, 2803–2817, doi:10.1016/j.atmosenv.2004.02.034, 2004.

Bian, H. and Prather, M.: Fast-J2: Accurate Simulation of Stratospheric Photolysis in Global Chemical Models, J. Atmos. Chem., 41, 281–296, doi:10.1023/A:1014980619462, 2002.

Breivik, Ø., Mogensen, K., Bidlot, J.-R., Balmaseda, M. A., and Janssen, P. A. E. M.: Surface wave effects in the NEMO ocean model: Forced and coupled experiments, J. Geophys. Res.-Oceans, 120, 2973–2992, doi:10.1002/2014JC010565, 2015.

Cakmur, R., Miller, R., and Torres, O.: Incorporating the effect of small-scale circulations upon dust emission in an atmospheric general circulation model, J. Geophys. Res., 109, D07201, doi:10.1029/2003JD004067, 2004.

Carrer, D., Ceamanos, X., Six, B., and Roujean, J.-L.: AERUSGEO: A newly available satellite-derived aerosol optical depth product over Europe and Africa, Geophys. Res. Lett., 41, 7731–7738, doi:10.1002/2014GL061707, 2014.

Dufresne, J.-L., Foujols, M.-A., Denvil, S., Caubel, A., Marti, O., Aumont, O., Balkanski, Y., Bekki, S., Bellenger, H., Benshila, R., Bony, S., Bopp, L., Braconnot, P., Brockmann, P., Cadule, P., Cheruy, F., Codron, F., Cozic, A., Cugnet, D., Noblet, N., Duvel, J.-P., Ethé, C., Fairhead, L., Fichefet, T., Flavoni, S., Friedlingstein, P., Grandpeix, J.-Y., Guez, L., Guilyardi, E., Hauglustaine, D., Hourdin, F., Idelkadi, A., Ghattas, J., Joussaume, S., Kageyama, M., Krinner, G., Labetoulle, S., Lahellec, A., Lefebvre, M.-P., Lefevre, F., Levy, C., Li, Z. X., Lloyd, J., Lott, F., Madec, G., Mancip, M., Marchand, M., Masson, S., Meurdesoif, Y., Mignot, J., Musat, I., Parouty, S., Polcher, J., Rio, C., Schulz, M., Swingedouw, D., Szopa, S., Talandier, C., Terray, P., Viovy, N., and Vuichard, N.: Climate change projections using the IPSL-CM5 Earth System Model: from CMIP3 to CMIP5, Clim. Dynam., 40, 2123–2165, doi:10.1007/s00382-012-1636-1, 2013.

Fogli, P. G. and Iovino, D.: CMCC-CESM-NEMO: toward the new CMCC Earth System Model, ANS – Numerical Applications and Scenarios Division, RP0248, 2014.

Folberth, G. A., Hauglustaine, D. A., Lathière, J., and Brocheton, F.: Interactive chemistry in the Laboratoire de Météorologie Dynamique general circulation model: model description and impact analysis of biogenic hydrocarbons on tropospheric chemistry, Atmos. Chem. Phys., 6, 2273–2319, doi:10.5194/acp-6-2273-2006, 2006.

Gasper, F., Goergen, K., Shrestha, P., Sulis, M., Rihani, J., Geimer, M., and Kollet, S.: Implementation and scaling of the fully coupled Terrestrial Systems Modeling Platform (TerrSysMP v1.0) in a massively parallel supercomputing environment – a case study on JUQUEEN (IBM Blue Gene/Q), Geosci. Model Dev., 7, 2531–2543, doi:10.5194/gmd-7-2531-2014, 2014.

Ginoux, P., Chin, M., Tegen, I., Prospero, J. M., Holben, B., Dubovik, O., and Lin, S. J.: Sources and distributions of dust aerosols simulated with the GOCART model, J. Geophys. Res., 106, 20255–20273, 2001.

Giorgetta, M. A., Jungclaus, J., Reick, C. H., Legutke, S., Bader, J., Böttinger, M., Brovkin, V., Crueger, T., Esch, M., Fieg, K., Glushak, K., Gayler, V., Haak, H., Hollweg, H.-D., Ilyina, T., Kinne, S., Kornblueh, L., Matei, D., Mauritsen, T., Mikolajewicz, U., Mueller, W., Notz, D., Pithan, F., Raddatz, T., Rast, S., Redler, R., Roeckner, E., Schmidt, H., Schnur, R., Segschneider, J., Six, K. D., Stockhause, M., Timmreck, C., Wegner, J., Widmann, H., Wieners, K.-H., Claussen, M., Marotzke, J., and Stevens, B.: Climate and carbon cycle changes from 1850 to 2100 in MPI-ESM simulations for the Coupled Model Intercomparison Project phase 5, J. Adv. Model. Earth Syst., 5, 572–597, doi:10.1002/jame.20038, 2013.

Grell, G. A. and Freitas, S. R.: A scale and aerosol aware stochastic convective parameterization for weather and air quality modeling, Atmos. Chem. Phys., 14, 5233–5250, doi:10.5194/acp-14-5233-2014, 2014.

Grell, G. A., Peckham, S. E., Schmitz, R., McKeen, S. A., Frost, G., Skamarock, W. C., and Eder, B.: Fully coupled "online" chemistry within the {WRF} model, Atmos. Environ., 39, 6957–6975, doi:10.1016/j.atmosenv.2005.04.027, 2005.

Guenther, A., Karl, T., Harley, P., Wiedinmyer, C., Palmer, P. I., and Geron, C.: Estimates of global terrestrial isoprene emissions using MEGAN (Model of Emissions of Gases and Aerosols from Nature), Atmos. Chem. Phys., 6, 3181–3210, doi:10.5194/acp-6-3181-2006, 2006.

Guo, J. and Yin, Y.: Mineral dust impacts on regional precipitation and summer circulation in East Asia using a regional coupled

climate system model, J. Geophys. Res.-Atmos., 120, 10378–10398, doi:10.1002/2015JD023096, 2015.

Han, Z., Li, J., Xia, X., and Zhang, R.: Investigation of direct radiative effects of aerosols in dust storm season over East Asia with an online coupled regional climate-chemistry-aerosol model, Atmos. Environ., 54, 688–699, doi:10.1016/j.atmosenv.2012.01.041, 2012.

Hansen, J., Sato, M., and Ruedy, R.: Radiative forcing and climate response, J. Geophys. Res.-Atmos., 102, 6831–6864, doi:10.1029/96JD03436, 1997.

Holben, B., Eck, T., Slutsker, I., Tanré, D., Buis, J., Setzer, A., Vermote, E., Reagan, J., Kaufman, Y., Nakajima, T., Lavenu, F., Jankowiak, I., and Smirnov, A.: AERONET – A Federated Instrument Network and Data Archive for Aerosol Characterization, Remote Sens. Environ., 66, 1–16, doi:10.1016/S0034-4257(98)00031-5, 1998.

Hourdin, F., Musat, I., Bony, S., Braconnot, P., Codron, F., Dufresne, J.-L., Fairhead, L., Filiberti, M.-A., Friedlingstein, P., Grandpeix, J.-Y., Krinner, G., LeVan, P., Li, Z.-X., and Lott, F.: The LMDZ4 general circulation model: climate performance and sensitivity to parametrized physics with emphasis on tropical convection, Clim. Dynam., 27, 787–813, doi:10.1007/s00382-006-0158-0, 2006.

Hsu, N. C., Jeong, M.-J., Bettenhausen, C., Sayer, A. M., Hansell, R., Seftor, C. S., Huang, J., and Tsay, S.-C.: Enhanced Deep Blue aerosol retrieval algorithm: The second generation, J. Geophys. Res.-Atmos., 118, 9296–9315, doi:10.1002/jgrd.50712, 2013.

Iacono, M. J., Delamere, J. S., Mlawer, E. J., Shephard, M. W., Clough, S. A., and Collins, W. D.: Radiative forcing by long-lived greenhouse gases: Calculations with the AER radiative transfer models, J. Geophys. Res.-Atmos., 113, d13103, doi:10.1029/2008JD009944, 2008.

Im, U., Bianconi, R., Solazzo, E., Kioutsioukis, I., Badia, A., Balzarini, A., Baró, R., Bellasio, R., Brunner, D., Chemel, C., Curci, G., Flemming, J., Forkel, R., Giordano, L., Jiménez-Guerrero, P., Hirtl, M., Hodzic, A., Honzak, L., Jorba, O., Knote, C., Kuenen, J. J., Makar, P. A., Manders-Groot, A., Neal, L., Pérez, J. L., Pirovano, G., Pouliot, G., Jose, R. S., Savage, N., Schroder, W., Sokhi, R. S., Syrakov, D., Torian, A., Tuccella, P., Werhahn, J., Wolke, R., Yahya, K., Zabkar, R., Zhang, Y., Zhang, J., Hogrefe, C., and Galmarini, S.: Evaluation of operational on-line-coupled regional air quality models over Europe and North America in the context of {AQMEII} phase 2. Part I: Ozone, Atmos. Environ., 115, 404–420, doi:10.1016/j.atmosenv.2014.09.042, 2015a.

Im, U., Bianconi, R., Solazzo, E., Kioutsioukis, I., Badia, A., Balzarini, A., Baró, R., Bellasio, R., Brunner, D., Chemel, C., Curci, G., van der Gon, H. D., Flemming, J., Forkel, R., Giordano, L., Jiménez-Guerrero, P., Hirtl, M., Hodzic, A., Honzak, L., Jorba, O., Knote, C., Makar, P. A., Manders-Groot, A., Neal, L., Pérez, J. L., Pirovano, G., Pouliot, G., Jose, R. S., Savage, N., Schroder, W., Sokhi, R. S., Syrakov, D., Torian, A., Tuccella, P., Wang, K., Werhahn, J., Wolke, R., Zabkar, R., Zhang, Y., Zhang, J., Hogrefe, C., and Galmarini, S.: Evaluation of operational online-coupled regional air quality models over Europe and North America in the context of {AQMEII} phase 2. Part II: Particulate matter, Atmos. Environ., 115, 421–441, doi:10.1016/j.atmosenv.2014.08.072, 2015b.

Jacob, R., Larson, J., and Ong, E.: M × N Communication and Parallel Interpolation in Community Climate System Model Version 3 Using the Model Coupling Toolkit, International Journal of High Performance Computing Applications, 19, 293–307, doi:10.1177/1094342005056116, 2005.

Jacobson, M. Z., Kaufman, Y. J., and Rudich, Y.: Examining feedbacks of aerosols to urban climate with a model that treats 3-D clouds with aerosol inclusions, J. Geophys. Res.-Atmos., 112, d24205, doi:10.1029/2007JD008922, 2007.

Jones, A., Roberts, D. L., and Slingo, A.: A climate model study of indirect radiative forcing by anthropogenic sulphate aerosols, Nature, 370, 450–453, doi:10.1038/370450a0, 1994.

Jungclaus, J. H., Fischer, N., Haak, H., Lohmann, K., Marotzke, J., Matei, D., Mikolajewicz, U., Notz, D., and von Storch, J. S.: Characteristics of the ocean simulations in the Max Planck Institute Ocean Model (MPIOM) the ocean component of the MPI-Earth system model, J. Adv. Model. Earth Syst., 5, 422–446, doi:10.1002/jame.20023, 2013.

Kahn, R. A., Gaitley, B. J., Martonchik, J. V., Diner, D. J., Crean, K. A., and Holben, B.: Multiangle Imaging Spectroradiometer (MISR) global aerosol optical depth validation based on 2 years of coincident Aerosol Robotic Network (AERONET) observations, J. Geophys. Res.-Atmos., 110, d10S04, doi:10.1029/2004JD004706, 2005.

Kalnay, E., Kanamitsu, M., Kistler, R., Collins, W., Deaven, D., Gandin, L., Iredell, M., Saha, S., White, G., Woollen, J., Zhu, Y., Chelliah, M., Ebisuzaki, W., Higgins, W., Janowiak, J., Mo, K., Ropelewski, C., Wang, J., Leetmaa, A., Reynolds, R., Jenne, R., and Joseph, D.: The NCEP/NCAR 40-year reanalysis project, B. Am. Meteorol. Soc., 77, 437–471, 1996.

Krinner, G., Viovy, N., de Noblet-Ducoudré, N., Ogée, J., Polcher, J., Friedlingstein, P., Ciais, P., Sitch, S., and Prentice, I. C.: A dynamic global vegetation model for studies of the coupled atmosphere-biosphere system, Global Biogeochem. Cy., 19, gB1015, doi:10.1029/2003GB002199, 2005.

Larson, J., Jacob, R., and Ong, E.: The Model Coupling Toolkit: A New Fortran90 Toolkit for Building Multiphysics Parallel Coupled Models, International Journal of High Performance Computing Applications, 19, 277–292, doi:10.1177/1094342005056115, 2005.

Levy, R., Hsu, C. et al.: MODIS Atmosphere L2 Aerosol Product, NASA MODIS Adaptive Processing System, available at: http://dx.doi.org/10.5067/MODIS/MOD04_L2.006, Goddard Space Flight Center, USA, 2015.

Li, J., keng Liao, W., Choudhary, A., Ross, R., Thakur, R., Gropp, W., Latham, R., Siegel, A., Gallagher, B., and Zingale, M.: Parallel netCDF: A High-Performance Scientific I/O Interface, SC Conference, 0, 39, doi:10.1109/SC.2003.10053, 2003.

Loosmore, G. and Cederwall, R.: Precipitation scavenging of atmospheric aerosols for emergency response applications: testing an updated model with new real-time data, Atmos. Environ., 38, 993–1003, 2004.

Madec, G.: NEMO ocean engine. Note du Pôle de modélisation, Institut Pierre-Simon Laplace (IPSL), France No 27 ISSN No 1288-1619, 2008.

Mailler, S., Menut, L., di Sarra, A. G., Becagli, S., Di Iorio, T., Bessagnet, B., Briant, R., Formenti, P., Doussin, J.-F., Gómez-Amo, J. L., Mallet, M., Rea, G., Siour, G., Sferlazzo, D. M., Traversi, R., Udisti, R., and Turquety, S.: On the ra-

diative impact of aerosols on photolysis rates: comparison of simulations and observations in the Lampedusa island during the ChArMEx/ADRIMED campaign, Atmos. Chem. Phys., 16, 1219–1244, doi:10.5194/acp-16-1219-2016, 2016a.

Mailler, S., Menut, L., Khvorostyanov, D., Valari, M., Couvidat, F., Siour, G., Turquety, S., Briant, R., Tuccella, P., Bessagnet, B., Colette, A., Létinois, L., and Meleux, F.: CHIMERE-2016: From urban to hemispheric chemistry-transport modeling, Geosci. Model Dev. Discuss., doi:10.5194/gmd-2016-196, in review, 2016b (data available at: http://www.lmd.polytechnique.fr/chimere/, last access: February 2017).

Maisonnave, E. and Caubel, A.: LUCIA, load balancing tool for OASIS coupled systems, TR-CMGC-14-63, available at: http://www.cerfacs.fr/globc/publication/technicalreport/2014/lucia_documentation.pdf (last access: February 2017), CERFACS, 2014.

Menut, L., Bessagnet, B., Khvorostyanov, D., Beekmann, M., Blond, N., Colette, A., Coll, I., Curci, G., Foret, G., Hodzic, A., Mailler, S., Meleux, F., Monge, J.-L., Pison, I., Siour, G., Turquety, S., Valari, M., Vautard, R., and Vivanco, M. G.: CHIMERE 2013: a model for regional atmospheric composition modelling, Geosci. Model Dev., 6, 981–1028, doi:10.5194/gmd-6-981-2013, 2013.

Menut, L., Mailler, S., Siour, G., Bessagnet, B., Turquety, S., Rea, G., Briant, R., Mallet, M., Sciare, J., Formenti, P., and Meleux, F.: Ozone and aerosol tropospheric concentrations variability analyzed using the ADRIMED measurements and the WRF and CHIMERE models, Atmos. Chem. Phys., 15, 6159–6182, doi:10.5194/acp-15-6159-2015, 2015.

Morrison, H., Thompson, G., and Tatarskii, V.: Impact of Cloud Microphysics on the Development of Trailing Stratiform Precipitation in a Simulated Squall Line: Comparison of One- and Two-Moment Schemes, Mon. Weather Rev., 137, 991–1007, doi:10.1175/2008MWR2556.1, 2009.

Nabat, P., Somot, S., Mallet, M., Michou, M., Sevault, F., Driouech, F., Meloni, D., di Sarra, A., Di Biagio, C., Formenti, P., Sicard, M., Léon, J.-F., and Bouin, M.-N.: Dust aerosol radiative effects during summer 2012 simulated with a coupled regional aerosol-atmosphere-ocean model over the Mediterranean, Atmos. Chem. Phys., 15, 3303–3326, doi:10.5194/acp-15-3303-2015, 2015.

Nakanishi, M. and Niino, H.: An Improved Mellor–Yamada Level-3 Model: Its Numerical Stability and Application to a Regional Prediction of Advection Fog, Bound.-Lay. Meteorol., 119, 397–407, doi:10.1007/s10546-005-9030-8, 2006.

Nakanishi, M. and Niino, H.: Development of an Improved Turbulence Closure Model for the Atmospheric Boundary Layer, Journal of the Meteorological Society of Japan. Ser. II, 87, 895–912, doi:10.2151/jmsj.87.895, 2009.

Nickovic, S., Kallos, G., Papadopoulos, A., and Kakaliagou, O.: A model for prediction of desert dust cycle in the atmosphere, J. Geophys. Res.-Atmos., 106, 18113–18129, doi:10.1029/2000JD900794, 2001.

Péré, J. C., Bessagnet, B., Mallet, M., Waquet, F., Chiapello, I., Minvielle, F., Pont, V., and Menut, L.: Direct radiative effect of the Russian wildfires and its impact on air temperature and atmospheric dynamics during August 2010, Atmos. Chem. Phys., 14, 1999–2013, doi:10.5194/acp-14-1999-2014, 2014.

Pérez, C., Nickovic, S., Pejanovic, G., Baldasano, J. M., and Özsoy, E.: Interactive dust-radiation modeling: A step to improve weather forecasts, J. Geophys. Res.-Atmos., 111, d16206, doi:10.1029/2005JD006717, 2006.

Péré, J. C., Mallet, M., Pont, V., and Bessagnet, B.: Impact of aerosol direct radiative forcing on the radiative budget, surface heat fluxes, and atmospheric dynamics during the heat wave of summer 2003 over western Europe: A modeling study, J. Geophys. Res.-Atmos., 116, d23119, doi:10.1029/2011JD016240, 2011.

Ramanathan, V., Crutzen, P. J., Lelieveld, J., Mitra, A. P., Althausen, D., Anderson, J., Andreae, M. O., Cantrell, W., Cass, G. R., Chung, C. E., Clarke, A. D., Coakley, J. A., Collins, W. D., Conant, W. C., Dulac, F., Heintzenberg, J., Heymsfield, A. J., Holben, B., Howell, S., Hudson, J., Jayaraman, A., Kiehl, J. T., Krishnamurti, T. N., Lubin, D., McFarquhar, G., Novakov, T., Ogren, J. A., Podgorny, I. A., Prather, K., Priestley, K., Prospero, J. M., Quinn, P. K., Rajeev, K., Rasch, P., Rupert, S., Sadourny, R., Satheesh, S. K., Shaw, G. E., Sheridan, P., and Valero, F. P. J.: Indian Ocean Experiment: An integrated analysis of the climate forcing and effects of the great Indo-Asian haze, J. Geophys. Res.-Atmos., 106, 28371–28398, doi:10.1029/2001JD900133, 2001.

Rea, G., Turquety, S., Menut, L., Briant, R., Mailler, S., and Siour, G.: Source contributions to 2012 summertime aerosols in the Euro-Mediterranean region, Atmos. Chem. Phys., 15, 8013–8036, doi:10.5194/acp-15-8013-2015, 2015.

Redler, R., Valcke, S., and Ritzdorf, H.: OASIS4 – a coupling software for next generation earth system modelling, Geosci. Model Dev., 3, 87–104, doi:10.5194/gmd-3-87-2010, 2010.

Samson, G., Masson, S., Lengaigne, M., Keerthi, M. G., Vialard, J., Pous, S., Madec, G., Jourdain, N. C., Jullien, S., Menkes, C., and Marchesiello, P.: The NOW regional coupled model: Application to the tropical Indian Ocean climate and tropical cyclone activity, J. Adv. Model. Earth Syst., 6, 700–722, doi:10.1002/2014MS000324, 2014.

Schmidt, H., Derognat, C., Vautard, R., and Beekmann, M.: A comparison of simulated and observed ozone mixing ratios for the summer of 1998 in western Europe, Atmos. Environ., 35, 6277–6297, 2001.

Shrestha, P., Sulis, M., Masbou, M., Kollet, S., and Simmer, C.: A Scale-Consistent Terrestrial Systems Modeling Platform Based on COSMO, CLM, and ParFlow, Mon. Weather Rev., 142, 3466–3483, 2014.

Skamarock, W., Klemp, J., Dudhia, J., Gill, D., Barker, D., Wang, W., and Powers, J.: A Description of the Advanced Research WRF Version 2, NCAR Technical Note, Boulder, Colorado, USA, NCAR/TN–468+STR, 2007 (data available at: http://www.wrf-model.org/index.php, last access: February 2017).

Sokolik, I. N. and Toon, O. B.: Direct radiative forcing by anthropogenic airborne mineral aerosols, Nature, 381, 681–683, doi:10.1038/381681a0, 1996.

Sterl, A., Bintanja, R., Brodeau, L., Gleeson, E., Koenigk, T., Schmith, T., Semmler, T., Severijns, C., Wyser, K., and Yang, S.: A look at the ocean in the EC-Earth climate model, Clim. Dynam., 39, 2631–2657, doi:10.1007/s00382-011-1239-2, 2012.

Stevens, B., Giorgetta, M., Esch, M., Mauritsen, T., Crueger, T., Rast, S., Salzmann, M., Schmidt, H., Bader, J., Block, K., Brokopf, R., Fast, I., Kinne, S., Kornblueh, L., Lohmann, U., Pincus, R., Reichler, T., and Roeckner, E.: Atmospheric component

of the MPI-M Earth System Model: ECHAM6, J. Adv. Model. Earth Syst., 5, 146–172, doi:10.1002/jame.20015, 2013.

Tewari, M., Chen, F., Wang, W., Dudhia, J., LeMone, M., Mitchell, K., Ek, M., Gayno, G., Wegiel, J., and Cuenca, R.: Implementation and verification of the unified NOAH land surface model in the WRF model., 20th conference on weather analysis and forecasting/16th conference on numerical weather prediction, 11–15, 2004.

Turquety, S., Menut, L., Bessagnet, B., Anav, A., Viovy, N., Maignan, F., and Wooster, M.: APIFLAME v1.0: high-resolution fire emission model and application to the Euro-Mediterranean region, Geosci. Model Dev., 7, 587–612, doi:10.5194/gmd-7-587-2014, 2014.

Valcke, S., Craig, T., and Coquart, L.: OASIS3-MCT User Guide, OASIS3-MCT 3.0, CERFACS/CNRS SUC URA No1875, 2015 (data available at: https://verc.enes.org/oasis, last access: February 2017).

Vogel, B., Vogel, H., Bäumer, D., Bangert, M., Lundgren, K., Rinke, R., and Stanelle, T.: The comprehensive model system COSMO-ART – Radiative impact of aerosol on the state of the atmosphere on the regional scale, Atmos. Chem. Phys., 9, 8661–8680, doi:10.5194/acp-9-8661-2009, 2009.

Voldoire, A., Sanchez-Gomez, E., Salas y Mélia, D., Decharme, B., Cassou, C., Sénési, S., Valcke, S., Beau, I., Alias, A., Chevallier, M., Déqué, M., Deshayes, J., Douville, H., Fernandez, E., Madec, G., Maisonnave, E., Moine, M.-P., Planton, S., Saint-Martin, D., Szopa, S., Tyteca, S., Alkama, R., Belamari, S., Braun, A., Coquart, L., and Chauvin, F.: The CNRM-CM5.1 global climate model: description and basic evaluation, Clim. Dynam., 40, 2091–2121, doi:10.1007/s00382-011-1259-y, 2013.

Wesely, M.: Parameterization of Surface Resistances to Gaseous Dry Deposition in Regional-Scale Numerical Models, Atmos. Environ., 23, 1293–1304, 1989.

Wild, O., Zhu, X., and Prather, M.: Fast-J: Accurate Simulation of In- and Below-Cloud Photolysis in Tropospheric Chemical Models, J. Atmos. Chem., 37, 245–282, doi:10.1023/A:1006415919030, 2000.

Williams, K. D., Harris, C. M., Bodas-Salcedo, A., Camp, J., Comer, R. E., Copsey, D., Fereday, D., Graham, T., Hill, R., Hinton, T., Hyder, P., Ineson, S., Masato, G., Milton, S. F., Roberts, M. J., Rowell, D. P., Sanchez, C., Shelly, A., Sinha, B., Walters, D. N., West, A., Woollings, T., and Xavier, P. K.: The Met Office Global Coupled model 2.0 (GC2) configuration, Geosci. Model Dev., 8, 1509–1524, doi:10.5194/gmd-8-1509-2015, 2015.

Wong, D. C., Pleim, J., Mathur, R., Binkowski, F., Otte, T., Gilliam, R., Pouliot, G., Xiu, A., Young, J. O., and Kang, D.: WRF-CMAQ two-way coupled system with aerosol feedback: software development and preliminary results, Geosci. Model Dev., 5, 299–312, doi:10.5194/gmd-5-299-2012, 2012.

Yu, H., Kaufman, Y. J., Chin, M., Feingold, G., Remer, L. A., Anderson, T. L., Balkanski, Y., Bellouin, N., Boucher, O., Christopher, S., DeCola, P., Kahn, R., Koch, D., Loeb, N., Reddy, M. S., Schulz, M., Takemura, T., and Zhou, M.: A review of measurement-based assessments of the aerosol direct radiative effect and forcing, Atmos. Chem. Phys., 6, 613–666, doi:10.5194/acp-6-613-2006, 2006.

Yue, X., Wang, H., Liao, H., and Fan, K.: Simulation of dust aerosol radiative feedback using the GMOD: 2. Dust-climate interactions, J. Geophys. Res.-Atmos., 115, d04201, doi:10.1029/2009JD012063, 2010.

Zhang, Y.: Online-coupled meteorology and chemistry models: history, current status, and outlook, Atmos. Chem. Phys., 8, 2895–2932, doi:10.5194/acp-8-2895-2008, 2008.